Hydrogen-bond imaging and engineering
with a scanning tunneling microscope

Hiroshi Okuyama[*]

Department of Chemistry, Graduate School of Science,

Kyoto University, Kyoto 606-8502, Japan

Ikutaro Hamada

WPI-Advanced Institute for Materials Research,

Tohoku University, Sendai 980-8577, Japan

(Dated: June 27, 2011)

Abstract

The scanning tunneling microscope (STM) has been a valuable tool in surface science for the study of structures and electronic states of metal surfaces. The recent advance of STM as a state-of-the-art technique to probe and manipulate individual molecules has made it possible to investigate molecular dynamics and chemical reactions at the surface in a single-molecule limit. In this review article, we present an overview of our recent work of H-bond imaging, manipulating and engineering at a metal surface. ¿From individual water molecules, a variety of H-bonded structures including water clusters, hydroxyl clusters and water-hydroxyl complexes are assembled on Cu(110), whose properties and dynamics are studied in real space in collaboration with density-functional-theory calculations.

PACS numbers:

[*]Electronic address: hokuyama@kuchem.kyoto-u.ac.jp

I. INTRODUCTION

Adsorption and reaction of water molecules on metal surfaces have been investigated extensively by both experiments and theories [1–4], toward the microscopic understandings of important surface phenomena, such as corrosion, electrode reactions and heterogeneous catalysis. The scanning tunneling microscope (STM) has been a useful tool for studying the overlayer growth of water on the surfaces. Water molecules form a variety of overlayers depending on the substrates, being stabilized in 2D [5–7] or 1D [8–10] network of H bonds. The structure is optimized by a delicate balance between water-substrate bonding and intermolecular bonding. The mixed water/hydroxyl overlayer on metal surfaces has been another focus of intensive studies using STM [11–13]. It was suggested that strong water-hydroxyl bonding in which the hydroxyl acts as a strong H-bond acceptor plays a crucial role in the optimal water/hydroxyl network formation [13]. While it is not necessarily straightforward to deduce molecular arrangement in the overlayers from the STM images, theoretical simulations and their comparison with the images have been proved to be helpful to infer the internal structure [8, 10, 13].

In contrast to the overlayer growth, adsorption of individual water molecules, hydroxyl groups and their interactions have been studied only scarcely to date, although they are of fundamental importance to understand the extended overlayer formation. The recent advance of low-temperature STM has made it feasible to image and manipulate individual molecules on metal surfaces for the study of diffusion and chemical reactions at the ultimate spatial resolution [14, 15]. Because water molecules favor clustering on metal surfaces, low temperature (below ∼40 K) is essential to reduce the mobility and to inhibit the aggregation for the imaging of monomer species. Diffusion and aggregation of individual molecules were sequentially imaged on Pd(111) at 40 K and the barrier for diffusion was determined to be 120 mV [6]. On noble metal surfaces, the interaction between water molecule and substrate is much weaker and consequently the surface temperature requires to be lower than ∼10 K for the imaging of stable water monomers. Water molecules are not stable even at 8 K on Cu(100) and a diffusing molecule was observed as a fractional image [16]. The barrier was estimated to be ∼20 meV which is much lower than that on the Pd surface. Nevertheless, a cyclic water hexamer, being stabilized by optimal H-bond interaction, can be observed on Cu(111) [17]. It was even possible to observe sequential growth of the hexamer to heptamer,

octamer, and nonamer, in which the competition between the ability of water molecules to bond to the substrate and to accept H bonds from other molecules was suggested to rationalize the structure of the small water clusters on this surface [18].

Apart from the motivation for detailed description of water-metal interactions, the ability of STM to image and manipulate individual water molecules on the surfaces allows one to "see" the on-going reactions and dynamics of H-bond systems, which is of great interest owing to the fundamental importance of H-bond chemistry in a broad range of scientific disciplines. This review provides an overview of our recent investigation of water molecules and their derivatives on Cu(110) by STM and DFT. Starting with isolated water molecules, we produce water clusters, hydroxyl clusters, and water-hydroxyl complexes, all in a controlled way by STM manipulation. The assembled structures serve as model systems to investigate H-bond dynamics in real space. The DFT calculations are essential to associate the images with the real structures of molecules and also to provide detailed insight into the dynamics. We demonstrate here the ability of STM combined with density-functional-theory (DFT) calculations to provide molecular-scale understandings of H-bonded systems on the surface.

II.   WATER MONOMER

Water molecules exist as isolated monomers on Cu(110) at 6 K due to the limited mobility, thus allowing stable imaging of individual molecules. Diffusion of water monomers was observed and induced by STM [19]. An STM image of a water monomer shows a round protrusion (Fig. 1a). From the relative position with coadsorbed CO molecules which are known to be on top of Cu atoms [21], a water molecule is located on top of a Cu atom. According to the DFT calculation, water molecules adsorb on slightly deviated top site with binding energy of 0.34 eV (Fig. 1b). Similar deviation was also reported by the previous calculations [22, 23]. The energy variation around the top site is believed to be generally small in the water-metal interaction [24], and therefore, the molecule is probably fluctuating around the top site and thus imaged in average just on the top site.

Water molecules migrate over the surface even at 6 K. A fractional image of the center molecule (Fig. 1a) indicates that the molecule hops along the [1$\bar{1}$0] direction (Cu row) when the tip scans along the line. The hopping motion is either thermally activated or tip-induced. The contribution of the latter depends on the tunneling condition. A typical

trace of the molecule is shown in Fig. 2a as a function of time. The tunneling current and sample bias voltage during the tracking are $I=0.5$ nA and $V_s=24$ mV, respectively. The traces are represented by the displacement from the original position in the $[1\bar{1}0]$ (red) and $[001]$ (blue) directions. The hopping motion is predominantly along $[1\bar{1}0]$ with a step of one atomic distance ($a_0=2.56$ Å). The time intervals between the hopping events were collected from many cycles of tracking experiments (Fig. 2b). The distribution is fitted by an exponential function whose decay constant is the mean residence time. A hopping rate, the inverse of the mean residence time, was determined to be 0.13 s^{-1} at $V_s=24$ mV. There is a current dependence in the hopping rate (inset of Fig. 2b). At low current, the rate is nearly constant at $\sim$0.1 s^{-1}, where the tip effect is negligible and the motion is thermally activated. Thus a water molecule thermally migrates along the atomic row with $R_0=0.1$ s^{-1} at 6 K. By assuming the pre-exponential factor $\nu_0\approx10^{13}$ s^{-1}, we estimate that $R_0=\nu_0\exp(-E_{dif}/k_BT)$ yields the barrier $E_{dif}\approx15$ meV. The hopping motion becomes tip-induced when current exceeds $\sim$0.5 nA. This is ascribed to tip-molecule attractive interaction that will be used for controlled water manipulation (shown below).

The hopping rate varies as a function of bias voltage. While the tip effect is negligible at $V_s=24$ mV and $I<\sim0.5$ nA, there is a tip-induced hopping at high voltage. The residence time of water molecule was determined as follows: The tip was positioned over a water molecule and a voltage pulse was applied during which the feedback was turned off. The tunneling current during the pulse shows abrupt decreases that correspond to the motion of the water molecule. Typical result is shown in the inset of Fig. 3a ($V_s=54$ mV). The first and second drops indicate the moments of hopping events to the first- and second-neighbor sites along the atomic row, respectively. The distribution of the times spent by a molecule just below the tip during the pulse, is fitted by a single exponential function in the same way as Fig. 2b. The hopping rate was obtained as a function of bias voltage (Fig. 3a) for H_2O (red circles) and D_2O (blue crosses). Below $\sim$40 mV, the rate is almost constant, where the motion is thermally activated. The rates increase by almost two orders of magnitude at $\sim$40-70 mV for both isotopes. The current dependence of the rates was investigated at $V_s=54$ mV, which is shown in Fig. 3b in a logarithmic scale. The contribution of thermal motion ($R_0=0.1$ s^{-1}) is subtracted to evaluate the rate of the induced motion. The slope of 1.0$\pm$0.1 suggests that the motion is induced via inelastic tunneling of single electron [25] with the reaction (hopping) yield of 3×10^{-8} per electron.

4

It has been argued that molecular motion is induced via anharmonic coupling with the excitation of molecular vibration (Fig. 4) [25–27]. Ueba and Persson studied the STM-induced hopping motion of a CO molecule on Pd(110) [27]. They showed that it was coupled to the excitation of the C-O stretch mode, and the hopping rate increased almost linearly with bias voltage above the threshold voltage corresponding to the C-O vibration energy. Accordingly, we fit the rate to a linear function and constant value above and below the threshold, respectively (red curve in Fig. 3a), and obtain the threshold voltage of 43 mV for H_2O. The threshold is tentatively ascribed to the excitation of the perpendicular H_2O-Cu stretch mode, which couples to the lateral motion (hindered-translation mode along $[1\bar{1}0]$) and excites the molecule to overcome the diffusion barrier.

While the STM-induced perturbation by inelastic vibrational excitation is almost free below V_s=43 mV, tip-molecule interaction due to proximity effect appears as the current increases (or the tip-molecule distance decreases), as shown in the inset of Fig. 2b. We can also manipulate a water molecule using this tip-molecule interaction (Fig. 5), as demonstrated in the manipulation of metal adatoms on Cu(211) [28]. The lateral manipulation is conducted by decreasing the tunnel resistance to ∼1 MΩ, which brings the tip close to a water molecule, and then the tip is laterally scanned at ∼1 Å per second in the $[1\bar{1}0]$ or $[\bar{1}10]$ direction with the feedback maintained. Typical trace of the tip height during the scan (Fig. 5c) indicates the manipulation in the "pulling" mode [28]. Using these manipulation techniques, we are able to construct a variety of H-bond systems, as shown in the following sections.

III.   WATER DIMER

A water dimer was produced from two monomers on Cu(110) and the dynamical behavior of its H bond was visualized with the STM [29]. A dimer was produced from two water monomers by controlled STM manipulation. Whereas spontaneous clustering is inhibited due to the low mobility of the monomers at 6 K, as shown in Fig. 1, the molecules can be moved along the Cu row ($[1\bar{1}0]$ direction) by STM as described in the previous section. Thus we can induce an encounter between monomers and produce a dimer. Alternatively, water dimers can be produced simply by increasing surface temperature to ∼20 K, at which monomers can migrate with sufficiently high mobility to be encountered.

The top right in Fig. 6a shows a typical image of $(H_2O)_2$. The dimer appears fractional; it is dynamically fluctuating between two equivalent configurations. The dimer is stable against dissociation but can be broken by a voltage pulse of ~0.3 V. The dynamical behavior of the dimer is strongly isotope dependent. The bottom left in Fig. 6a shows an image of $(D_2O)_2$. These assignments are conducted by separate experiments using H_2O or D_2O, while the image of Fig. 6a was recorded in an isotope-mixed experiment [30]. In contrast to the H_2O dimer, the D_2O dimer appears stationary. It shows an asymmetric "egg" shape with the long axis oriented along the Cu row. The asymmetry is also discernible for each envelope of the fluctuating bistable image of the H_2O dimer. The D_2O dimer is also fluctuating but with much slower rate, and therefore it could be observed as a stationary image. The slow fluctuation of $(D_2O)_2$ is shown in Figs. 6b-6d. The dimer flips between two equivalent configurations of Figs. 6b and 6d.

The structure of an adsorbed water dimer was calculated by DFT, as shown in Figs. 7a (side view) and 7b (top view). The lower-lying molecule (H-bond donor) is directly bonded to the Cu atom, while the higher-lying molecule (H-bond acceptor) interacts weakly with the substrate. Similar structures have been proposed for water dimers on close-packed metallic surfaces [18, 31, 32]. The STM simulation for this structure (Fig. 7d) is characterized by the large and small protrusions over the acceptor and donor molecules, respectively. The simulation well reproduces the experimental $(D_2O)_2$ image (Fig. 7c). The schematic structure of a water dimer is superimposed on the image. Thus the bistable fluctuation shown in Figs. 6b-6d indicates the exchange of the roles as H-bond donor and acceptor in a water dimer. The H-bond interchange was proposed to cause the unexpectedly rapid diffusion of a water dimer on Pd(111) [6, 31].

The temporal evolution of the interchange motion was studied by monitoring the tunneling current over the dimer with the feedback turned off (Fig. 8a). The jumps in the current correspond to the individual interchange events within the dimer. The distribution of the time intervals between the events obtained at three different tunneling currents show the same slope in semi-logarithmic scale (Fig. 8b), indicating that the tip effect on the interchange motion is negligible at V_s=24 mV and I¡0.7 nA. The slopes indicate the rate of the interchange [$(6.0\pm0.6)\times10^1$ s^{-1} for $(H_2O)_2$]. The rate for $(D_2O)_2$ is determined in a similar way to be 1.0 ± 0.1 s^{-1}. The large isotope effect (~60) suggests that the rate-limiting process involves quantum tunneling. The interchange tunneling manifests for gas-phase wa-

6

ter dimers as tunneling splittings corresponding to $\sim 10^9$ s^{-1} for (H$_2$O)$_2$. The barrier to the interchange was calculated to be 23 kJ/mol [29], which is much larger than that for a free dimer (2.48 kJ/mol [33]). The interaction of water molecules with the surface increases the barrier height and thus reduces the interchange rate by seven orders of magnitude.

The interchange rate was determined as a function of V_s (Fig. 8c). While the interchange motion is intrinsic at low bias voltage (constant rate), it is induced by tunneling electrons at voltages higher than ~ 40 mV. The threshold voltage was determined to be 45±1(41±1) mV for H$_2$O (D$_2$O) dimers. The isotope effect (~ 1.1) suggests that inelastic vibrational excitation by tunneling electrons is responsible for the induced motion. Based on the normal-mode analysis, the donor-substrate stretch (inset in Fig. 8d) is assigned to the vibrational mode for this motion. This mode *directly* correlates with the interchange reaction coordinate, because the interchange motion involves the vertical displacement of oxygen atoms. This is in contrast to the case of Fig. 4, where the molecular motion is induced *indirectly* via coupling between vibrational modes. The barrier to the interchange is calculated to be 0.24 eV, which is much larger than the energy transferred from a tunneling electron (45 meV), and thus, the electron-induced interchange has to proceed through tunneling. Figure 8d shows a schematic diagram of the potential energy along the interchange pathway. We propose that the interchange tunneling is assisted by the vibrational excitation (red arrows). The mechanism of vibration-assisted tunneling was extended [34] to rationalize the STM-induced motion of Co atom on Cu(111) [35].

IV. WATER TRIMER AND TETRAMER

Larger clusters of trimer to hexamer were sequentially produced by adding a molecule step by step, and their structures were investigated in the light of DFT calculations [36]. A water trimer was produced from a monomer and a dimer located on the same Cu row. The trimer is imaged as an asymmetric triangle in one of the four equivalent configurations (Figs. 9a-9d). Because this trimer is yielded from a monomer and a dimer along the same Cu row, water molecules are arranged in a chain along the Cu row. The corresponding structures optimized by the DFT calculation are shown in the right part of Fig. 9. In analogy with the dimer (Fig. 7), the acceptor molecule is expected to show higher protrusion in the image. A cyclic trimer observed in gas phase [37] and proposed on Pt(111) [32] was not observed and

therefore is unfavorable when adsorbed on Cu(110) in spite of its maximized number of H bonds. Adsorption of a water cluster requires optimum adsorption sites wherein the energy gain both from water-water and water-substrate interaction is maximized; the adsorption geometry is determined by a delicate balance of these interactions. The cyclic form cannot find an optimum site, presumably because of the geometrical constraint of the quasi-1D Cu(110) surface.

In a similar way, the trimer was extended to a chain tetramer by adding a molecule to the end. A chain tetramer appears as a distorted-parallelogram protrusion (Fig. 10a). The optimized structure for the chain tetramer is shown in Fig. 10d. The distortion reflects the end molecules bonding as a single donor or an acceptor. Several isomers were observed for the tetramer on Cu(110). Typically two isomers are shown in Figs. 10b and 10c, characterized by a triangle and round images, respectively. The three isomers (chain, triangle and round) interconvert between each other by voltage pulses at $\sim$0.2 V. Figure 11 shows a series of images that illustrate the conversion from the chain to round isomers under the scan at V_s=133-143 mV. The round isomer is assigned to the cyclic configuration (Fig. 10f), while the triangle isomer is assigned to the tetrahedral configuration with the center molecule acting as a double donor and single acceptor (Fig. 10e). Similar configuration to the latter was predicted to exist on other surfaces [38, 39]. The calculated binding energies for these isomers are 0.49, 0.49 and 0.51 eV/H_2O for the chain, tetrahedral and cyclic structures, respectively. Thus, the cyclic form with maximal H bonds is the most favorable for the tetramer, indicating the crossover from chain (trimer) to cyclic (tetramer) configurations as the constituent number increases. This behavior of water clusters on Cu(110) is quite different from that of gas-phase counterparts [37] and on other surfaces [23, 38, 39], highlighting the decisive role of the underlying substrate in the clustering of small number of water molecules.

V. HYDROXYL GROUP

The STM was used not only to assemble water clusters but also to break O-H covalent bonds of a water molecule to yield hydroxyl (OH) species and oxygen atom on Cu(110) [40]. The bond breaking was conducted by applying voltage pulses of V_s=1.5-2.0 V to a water molecule or hydroxyl species with the STM. A voltage pulse of V_s=2 V for 0.5 s was enough

to dissociate a water molecule, and typical STM image of the product is shown in Fig. 12a. They are each imaged as paired depressions aligned along [001].

The assignment of these products as hydroxyl species is based on the vibrational characterization by inelastic electron tunneling spectroscopy (IETS) [41]. The IETS showed a peak at 58 and 41 mV for OH and OD, respectively, which are ascribed to the bending mode of hydroxyl groups [40]. ¿From the relative position to water molecules located on top of Cu atoms, the hydroxyl group (the center of the paired depressions) was determined to be located at the short-bridge site of Cu(110), in agreement with the previous studies [42, 43].

The assignment is reconfirmed by further dissociating it to an atomic oxygen. The tip was positioned over one of the products (top left in Fig. 12a) and a 0.9 V pulse was applied. The image after the pulse (Fig. 12b) shows that it has been dissociated into atomic oxygen imaged as a round and featureless depression [44]. The dissociation of OH to O is schematically shown in Fig. 12c. In either case of dissociation, detached H(D) atoms were not observed on the nearby surface, in contrast to dissociated H(D) atoms on Cu(100) [45]. The potential energy of H(D) atoms may be less corrugated along the Cu(110) surface, and consequently H(D) atoms are delocalized along the surface even in their (vibrationally) ground state [46].

Why is a hydroxyl group imaged as a pair of depressions along [001]? To answer this question, we calculated the binding structure of OH on Cu(110) (Fig. 13a). The OH group adsorbs on the short-bridge site via O atom with the axis inclined along [001]. Besides, the potential energy surface of OH along the lateral coordinates of H atom was calculated (Fig. 13b). The two minima correspond to the inclined geometries, and the molecule can flip via the transition state of upright geometry. It flips back and forth via tunneling through the barrier, and therefore the two depressions in the STM image of a OH group result from the fast flip motion of the inclined axis.

The flip motion of OD was observed in real time as two-state fluctuation in the tunneling current recorded with the tip fixed over the depression (Fig. 13c). The fluctuation is ascribed to the flip motion between two equivalent orientations of OD (Fig. 13d). No such fluctuation was observed for OH. The high-(low-)current states are tentatively assigned to the orientations of D atom near (away from) the tip. On the other hand, such fluctuation was not observed for OH, suggesting that the flip motion is much faster than OD and thus the associated fluctuation is smeared out due to the limited bandwidth of the preamplifier.

9

More recent DFT work revealed that the nuclear quantum effect of the oxygen atom is important to describe accurately the tunneling dynamics of this flip motion [47].

VI.   HYDROXYL CLUSTERS

By using the manipulation technique demonstrated in Fig. 5, a water molecule was reacted with an oxygen atom on Cu(110) to produce a hydroxyl dimer, as represented by $H_2O+O \rightarrow (OH)_2$ [40]. A water molecule (left in Fig. 14a) was dragged in the $[1\bar{1}0]$ direction to an oxygen atom (top right). The reaction occurs spontaneously between them when they come close to each other. The reaction product appears as a semicircular depression (Fig. 14b). Hydrogen peroxide species is ruled out by vibrational spectroscopy (shown below) as well as by DFT calculations which show that a peroxide molecule adsorbed on a Cu(110) surface spontaneously dissociates into an $(OH)_2$ dimer. This reaction process is schematically shown in Fig. 14c. The two OH groups are bound in the short-bridge sites on adjacent Cu rows and inclined along [001] to form a H bond between them.

The OH dimer is imaged as either of the two equivalent tautomers. While the isolated OH group is dynamically flipped between the two orientations, the images of a hydroxyl dimer indicate that the flip motion is quenched. It is stabilized by a H-bond between two OH groups, increasing the barrier to the flip and thus quenching the motion. Although the intrinsic motion is quenched, the OH dimers are induced to flip by tunneling electrons, as shown in Figs. 15a-15c. The asterisk in Figs. 15b and 15c shows the center of the flip motion located on the hollow site. Two-state fluctuation was observed in the tunneling current when the tip was fixed over $(OD)_2$ at V_s=303 mV (Fig. 16a). The fluctuation is associated with the back-and-forth flip motion of the dimer. The flip motion is enhanced by vibrational excitation and consequently causes a nonlinear feature at specific voltage in the averaged I-V curve (Fig. 16b, indicated by a downward arrow). The non-linearity is explicitly seen in the first derivative (dI/dV) as a peak at ∼300 mV (inset of Fig. 16b). This feature results from voltage-dependent preference of the high state to the low state in the two-state fluctuation [40, 48]. The tunneling current at the high and low states, together with their fractional occupation, were obtained as a function of the voltage (Fig. 16c). Using these data, the averaged I-V curve, represented by $I_{ave}=O_{high} \cdot I_{high}+O_{low} \cdot I_{low}$, where $O_{high(low)}$ and $I_{high(low)}$ are fractional occupations for high (low) states and tunneling current

10

at high (low) states, respectively, well reproduces the experimental data (circles in Fig. 16d). The nonlinear feature is ascribed to the abrupt changes in the fractional occupations, and its onset voltage is determined to be 290 mV from the peak in the d^2I/dV^2 (Fig. 18, bottom). The peak position shifts to 394 mV for $(OH)_2$. The peak voltage and the isotope shift suggest that the motion is induced by O-H(O-D) stretch excitation, as a result of the intermode coupling illustrated in Fig. 4. The vibrational energy is significantly red-shifted from that for free OH (443 meV for OH [49]). This spectroscopic data provide an evidence for H-bonding interaction in the produced hydroxyl dimers.

In a similar way, OH groups are assembled into longer chains, i.e., $(OH)_3$ and $(OH)_4$. The assembly process of $(OH)_4$ is shown in Fig. 17. First, two oxygen atoms are adsorbed so that they are apart from each other by $2b_0$ (b_0=3.54 Å is the Cu atomic distance along [001]) along the [001] direction (Fig. 17a). Then two water molecules are successively reacted with oxygen atoms (Figs. 17b and 17c), giving rise to an $(OH)_4$ chain along the [001] direction. In a similar way as $(OH)_2$, these OH chains are induced to flip by tunneling electrons and the corresponding d^2I/dV^2 shows peak-and-dip features associated with vibrational excitation of the O-H stretch (Fig. 18). Notably, the O-H stretch frequency of $(OH)_3$ (419 mV) is exceptionally higher than that of $(OH)_2$ (394 mV) and $(OH)_4$ (399 mV). Because O-H frequency is lowered by H-bonding O-H$\cdots$O, the higher frequency indicates weaker H bonding. The structures of $(OH)_2$, $(OH)_3$ and $(OH)_4$ are optimized by DFT (Fig. 19). $(OH)_2$ is stabilized by H bonding with the two OH groups bonded to the adjacent bridge sites along [001]. The two OH groups are displaced from the exact short-bridge site and reoriented to make the optimal configuration for H-bonding interaction. $(OH)_4$ is nearly dimerized, in which the two $(OH)_2$ units are weakly interacted with each other. On the other hand, the center molecule in $(OH)_3$ is "suspended" between two OH groups, and as a result, the H-bonding interaction in $(OH)_3$ is reduced as compared to that in $(OH)_2$ and of each $(OH)_2$ unit in $(OH)_4$. This is supported by the total energy calculations: Binding energy for $(OH)_3$ is 47 meV/OH with respective to isolated OH monomers on Cu(110), which is lower than 87 and 94 meV/OH those for $(OH)_2$ and $(OH)_4$, respectively, suggesting that OH groups in $(OH)_3$ is less stable than those in $(OH)_2$ and $(OH)_4$. Thus the OH chains favor dimerization, which is attributed to the strong-acceptor nature the OH group.

VII. WATER-HYDROXYL COMPLEXES

The manipulation of a water molecule demonstrated in Fig. 5 was also used to form an H bond between an OH group and a water molecule [50]. Figures 20a and 20b show sequential images before and after the reaction of a water molecule with an OH group on Cu(110), respectively. The water molecule and OH group are bonded to the on-top and short-bridge sites, respectively, on the adjacent row (Fig. 20c). The water molecule is induced to be encountered with the OH group, giving rise to an "oval"-shape product (Fig. 20b). The two dashed lines represent the Cu rows on which each reactant molecule is located, and the asterisk shows the center position of the original OH group (short-bridge site). The reaction occurs spontaneously when the reactants come close to each other. The product was never dissociated spontaneously once it was formed, suggesting the formation of a stable H-bonded complex. The image of the complex is shown with the substrate lattice superimposed (Fig. 20d). The line profiles of the image (Fig. 20e) suggest that the product has two mirror planes parallel to the $[1\bar{1}0]$ or $[001]$ axis and is therefore of C_{2v} symmetry.

The structures of the water-hydroxyl complex is optimized by DFT (Fig. 21a). The complex consists of water and OH group on the adjacent rows, that is stabilized by 0.44 eV with respect to the isolated species on the surface. The asymmetric structure in Fig. 21a seems, however, incompatible with the apparent C_{2v} symmetry of the oval complex. This contradiction is solved by taking into account the zero-point nuclear motion of the shared proton which is proposed to be delocalized between two oxygen atoms, yielding a centrosymmetric configuration. The adiabatic potential energy for the shared proton as it is transferred between the two oxygen atoms is shown in Fig. 21b (circles). The potential has a double-well structure with a significantly reduced barrier (16 meV) and small distance (0.2 Å) between the minima. The potential energy for the symmetric configuration is only 16 meV higher than that for the asymmetric configuration. The optimized O-O distance (2.5 Å) and the strong H-bond interaction (0.44 eV) are in line with the "low-barrier hydrogen bond" which has been proposed to explain proton transfer through an H bond in enzymic catalysis [51, 52]. The strong interaction is ascribed to the ability of an OH group to accept an H atom (proton) from a water molecule. Therefore it is likely that the zero-point motion gives rise to the stabilization of the symmetric configuration. Based on this idea, the zero-point energies are calculated and the total energies for the asymmetric and symmetric

configurations are compared. Indeed the total energy of the symmetric configuration is lower than that of the asymmetric one [50]. This suggests barrierless motion of shared H atom and thus formation of a symmetric H bond. The delocalized nature of shared proton (H atom) in water-hydroxyl overlayers was also proposed on close-packed transition metal surfaces [53], suggesting that the symmetric H bond as observed here is a general phenomenon in the water-hydroxyl bonding on metal surfaces and thus plays a key role in diverse redox processes.

VIII.   CONCLUDING REMARKS

The ability of STM to image and manipulate individual water molecules have made it possible to assemble a variety of H-bond systems in a well-defined environment and to probe their properties and dynamics in real space, such as H-bond interchange tunneling in a water dimer, single-proton flip in an OH group, and H-bond symmetrization in a water-OH complex. Combined with DFT calculations, it is possible to determine the real structure of molecules, which otherwise is only speculated. Furthermore, the potential-energy calculation provides detailed insight into the dynamics of individual molecules. Studying individual H-bonds provides an insight into optimal overlayer formation, but a combined approach of STM and DFT, as demonstrated here, is anticipated to provide detailed description of more complex H-bond systems which can serve as model systems for heterogeneous catalysis and electrode reactions.

[1] P.A. Thiel and T.E. Madey, Surf. Sci. Rep. **7**, 211 (1987).

[2] M.A. Henderson, Surf. Sci. Rep. **46**, 1 (2002).

[3] A. Verdaguer, G.M. Sacha, H. Bluhm and M. Salmeron, Chem. Rev. **106**, 1478 (2006).

[4] A. Hodgson and S. Haq, Surf. Sci. Rep. **64**, 381 (2009).

[5] M. Morgenstern, T. Michely and G. Comsa, Phys. Rev. Lett. **77**, 703 (1996); M. Morgenstern et al., Z. Phys. Chem. **198**, 43 (1997).

[6] T. Mitsui, M.K. Rose, E. Fomin, D.F. Ogletree, and M. Salmeron, Science **297**, 1850 (2002).

[7] A. Beniya, Y. Sakaguchi, T. Narushima, K. Mukai, Y. Yamashita, S. Yoshimoto, and J. Yoshinobu, J Chem. Phys. **130**, 034706 (2009).

[8] J. Cerda et al., Phys. Rev. Lett. **93**, 116101 (2004).

[9] T. Yamada, S. Tamamori, H. Okuyama and T. Aruga, Phys. Rev. Lett. **96**, 036105 (2006).

[10] J. Carrasco, A. Michaelides, M. Forster, S. Haq, R. Raval and A. Hodgson, Nature Mater. **8**, 427 (2009).

[11] M. Tatarkhanov, E. Fomin, M. Salmeron, K. Andersson, H. Ogasawara, L.G.M. Pettersson, A. Nilsson and J. Cerda, J. Chem. Phys. **129**, 154109 (2008).

[12] J. Lee, D.C. Sorescu, K.D. Jordan, and J.T. Yates, J. Phys. Chem. C**112**, 17672 (2008).

[13] M. Forster, R. Raval, A. Hodgson, J. Carrasco, and A. Michaelides, Phys. Rev. Lett. **106**, 046103 (2011).

[14] W. Ho, J. Chem. Phys. **117**, 11033 (2002).

[15] T. Komeda, Prog. Surf. Sci. **78**, 41 (2005).

[16] L. Lauhon and W. Ho, J. Phys. Chem. B**105**, 3987 (2001).

[17] K. Morgenstern and K.-H. Rieder, J. Chem. Phys. **116**, 5746 (2002).

[18] A. Michaelides and K. Morgenstern, Nature materials **6**, 597 (2007).

[19] T. Kumagai, M. Kaizu, H. Okuyama, S. Hatta, T. Aruga, I. Hamada, Y. Morikawa, e-J. Surf. Sci. Nanotech. **6**, 296 (2008).

[20] K. Motobayashi, C. Matsumoto, Y. Kim and M. Kawai, Surf. Sci. **602**, 3136 (2008).

[21] M. Doering, J. Buisset, H.-P. Rust, B.G. Briner and A.M. Bradshaw, Faraday Discuss. **105**, 163 (1996).

[22] Q.-L. Tang and Z.-X. Chen, Surf. Sci. **601**, 954 (2007).

[23] J. Ren and S. Meng, Phys. Rev. B**77**, 054110 (2008).

[24] A. Michaelides, V.A. Ranea, P.L. de Andres and D.A. King, Phys. Rev. Lett. **90**, 216102 (2003).

[25] B.C. Stipe, M.A. Rezaei and W. Ho, Phys. Rev. Lett. **81**, 1263 (1998).

[26] T. Komeda, Y. Kim, M. Kawai, B.N.J. Persson and H. Ueba, Science **295**, 2055 (2002).

[27] H. Ueba and B.N.J. Persson, Phys. Rev. B**75**, 041403(R) (2007).

[28] L. Bartels, G. Meyer, K.-H. Rieder, Phys. Rev. Lett. **79**, 697 (1997).

[29] T. Kumagai, M. Kaizu, S. Hatta, H. Okuyama, T. Aruga, I. Hamada, Y. Morikawa, Phys. Rev. Lett. **100**, 166101 (2008).

[30] In H_2O-D_2O-mixed experiments, dimer species with much slower motion ($\sim$0.1 s^{-1}) are observed. This dimer shows asymmetric motion with one configuration preferred, and thus is assigned as an H_2O-D_2O dimer.

[31] V.A. Ranea, A. Michaelides, R. Ramírez, P.L. de Andres, J.A. Vergés, and D.A. King, Phys. Rev. Lett. **92**, 136104 (2004).

[32] S. Meng, E.G. Wang, and S. Gao, Phys. Rev. B**69**, 195404 (2004).

[33] R.S. Fellers, C. Leforestier, L.B. Braly, M.G. Brown, and R.J. Saykally, Science **284**, 945 (1999).

[34] S.G. Tikhodeev and H. Ueba, Phys. Rev. Lett. **102**, 246101 (2009).

[35] A. Stroscio and R.J. Celotta, Science **306**, 242 (2004).

[36] T. Kumagai, H. Okuyama, S. Hatta, T. Aruga, and I. Hamada, J. Chem. Phys. **134**, 024703 (2011).

[37] N. Pugliano and R.J. Saykally, Science **257**, 1937 (1992).

[38] D. Sebastiani and L. Delle Site, J. Chem. Theory Comput. **1**, 78-82 (2005).

[39] A. Michaelides, Faraday Discuss. **136**, 287 (2007).

[40] T. Kumagai, M. Kaizu, H. Okuyama, S. Hatta, T. Aruga, I. Hamada and Y. Morikawa, Phys. Rev. B**79**, 035423 (2009).

[41] B.C. Stipe, M.A. Rezaei, and W. Ho, Science **280**, 1732 (1998).

[42] M. Polak, Surf. Sci. **321**, 249 (1994).

[43] Q.-L. Tang and Z.-X. Chen, J. Chem. Phys. **127**, 104707 (2007).

[44] B.G. Briner, M. Doering, H.-P. Rust, and A.M. Bradshaw, Phys. Rev. Lett. **78**, 1516 (1997).

[45] L.J. Lauhon, and W. Ho, Phys. Rev. Lett. **85**, 4566 (2000).

[46] M. Nishijima, H. Okuyama, N. Takagi, T. Aruga, and W. Brenig, Surf. Sci. Rep. **57**, 113 (2005).

[47] E.R.M. Davidson, A. Alavi, and A. Michaelides, Phys. Rev. B**81**, 153410 (2010).

[48] J. Gaudioso, L.J. Lauhon, and W. Ho, Phys. Rev. Lett. **85**, 1918 (2000).

[49] G. Herzberg, *Molecular Spectra and Molecular Structure I, Spectra of Diatomic Molecules* (Van Nostrand, Princeton, 1950).

[50] T. Kumagai, M. Kaizu, S. Hatta, H. Okuyama, T. Aruga, I. Hamada and Y. Morikawa, Phys. Rev. B**81**, 045402 (2010).

[51] W.W. Creland and M.M. Kreevoy, Science **264**, 1887 (1994).

[52] P.A. Frey, S.A. Whitt, and J.B. Tobin, Science **264**, 1927 (1994).

[53] X.-Z. Li, M.I.J. Probert, A. Alavi and A. Michaelides, Phys. Rev. Lett. **104**, 066102 (2010).
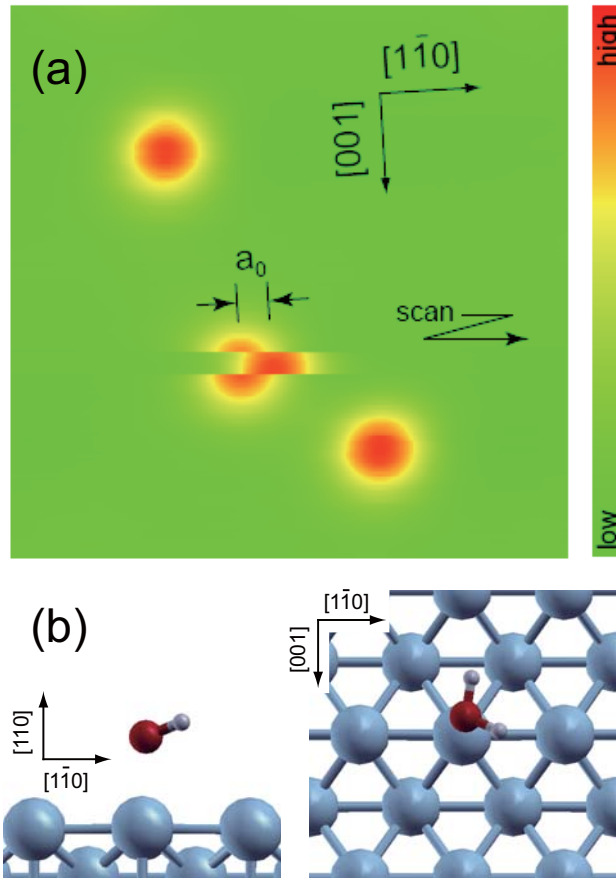
FIG. 1: (a) Typical STM images of water monomers on Cu(110) (V_s=24 mV and I=0.5 nA, 43×43 Å^2). Water molecules appear as round protrusions with apparent height of 0.6 Å. The tip is scanned horizontally from top to bottom. The fractional image of the center molecule indicates the hopping along the Cu row by a_0 (a_0=2.56 Å is the Cu-Cu distance along the [1$\bar{1}$0] direction). (b) Calculated structure of a water monomer on Cu(110).
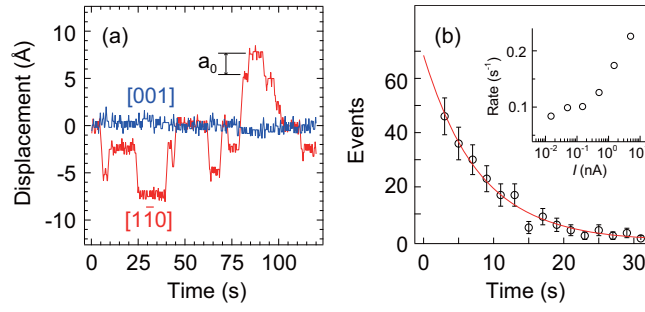
FIG. 2: (a) Typical trace of the tip when it tracks a water molecule at 24 mV and 0.5 nA. The red and blue lines indicate the displacements in the $[1\bar{1}0]$ and $[001]$ directions, respectively. (b) Distribution of the time intervals between the hopping events collected from the tracking data. The tunnel conditions are the same as in (a). The fitting to an exponential function gives a hopping rate of 0.13 s^{-1}. The inset shows the hopping rates as a function of current at V_s=24 mV. The tip effect is negligible at low current, and the residual rate (0.1 s^{-1}) is mainly ascribed to the thermal motion. (From [19].)
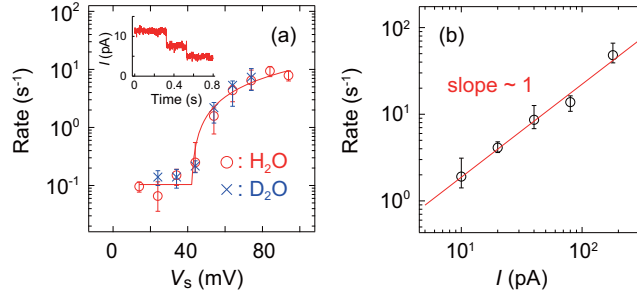
FIG. 3: (a) Hopping rates as a function of V_s for H_2O (red circles) and D_2O (blue crosses). The tip height is adjusted to give I=12±3 pA during the voltage pulses. The inset shows typical tunneling current taken with the tip fixed over the molecule at V_s=54 mV. (b) The rate of induced motion as a function of current at V_s=54 mV gives a slope of 1.0±0.1 in a logarithmic scale. (From [19].)

19
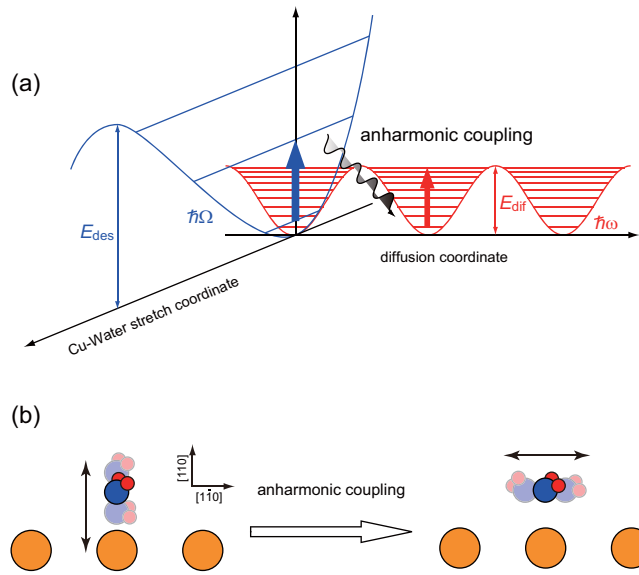
FIG. 4: Schematic diagram showing the STM-induced diffusion of a water molecule via the anharmonic coupling of H_2O-Cu stretch excitation ($\hbar\Omega$) with the hindered-translation mode ($\hbar\omega$). (a) E_{des} and E_{dif} represent the barriers to desorption and diffusion, respectively. (b) Schematic illustration of the stretch mode and hindered-translation mode.
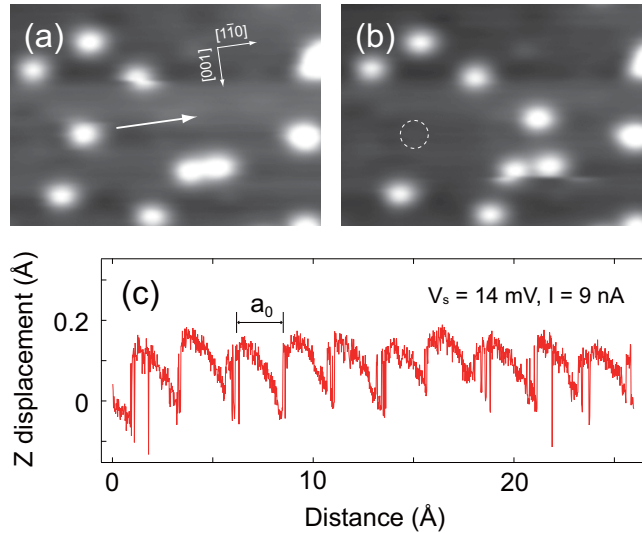
FIG. 5: (a),(b) Sequential STM images before and after a water molecule in the left center is manipulated along the $[1\bar{1}0]$ direction (along the arrow) with the tunnel resistance of $\sim$1 MΩ. (c) Typical Z (tip height) motion during the manipulation shows that the water molecule is "pulled" by the tip. The image size is 117$\times$84 Å^2, and the images are recorded at V_s=24 mV and I=0.5 nA.

20
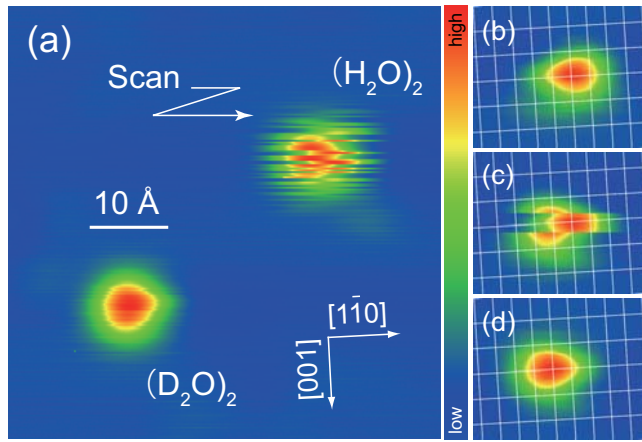
FIG. 6: (a) STM images of $(H_2O)_2$ and $(D_2O)_2$ on Cu(110) recorded at V_s=24 mV and I=0.5 nA (55×55 Å^2). The two isotopomers appear to be quite different from each other due to higher mobility (fluctuation) of $(H_2O)_2$. (b) An STM image of $(D_2O)_2$. Because $(D_2O)_2$ fluctuates slowly, it is imaged while it stays in one of the two configurations. (c) $(D_2O)_2$ flips twice during the scanning across it. (d) The counterpart of (b). The lines represent the lattice of Cu(110). The images (b)-(d) are recorded at V_s=24 mV and I=0.3 nA (24×20 Å^2). (From [29].)
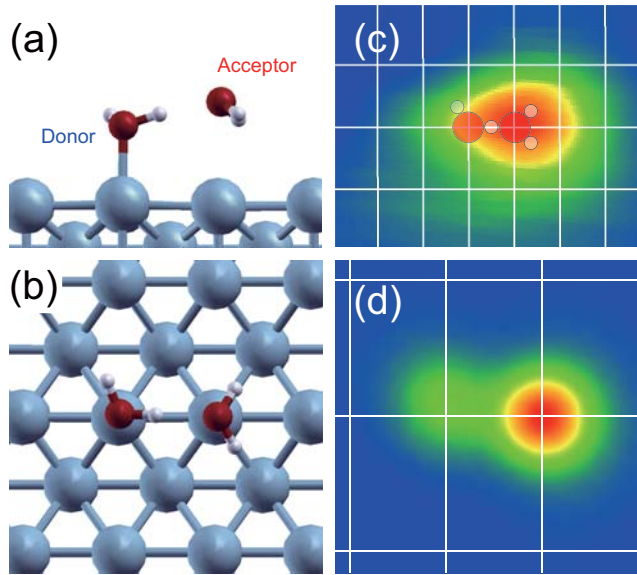
FIG. 7: (a) Side view and (b) top view of the structure of a water dimer on Cu(110). (c) An STM image of $(D_2O)_2$ recorded at V_s=24 mV and I=0.5 nA. (d) The simulated STM image for (b). The calculation well reproduces the experimental feature. In (c), the schematic structure of a dimer is superimposed on the experimental image. (From [29].)
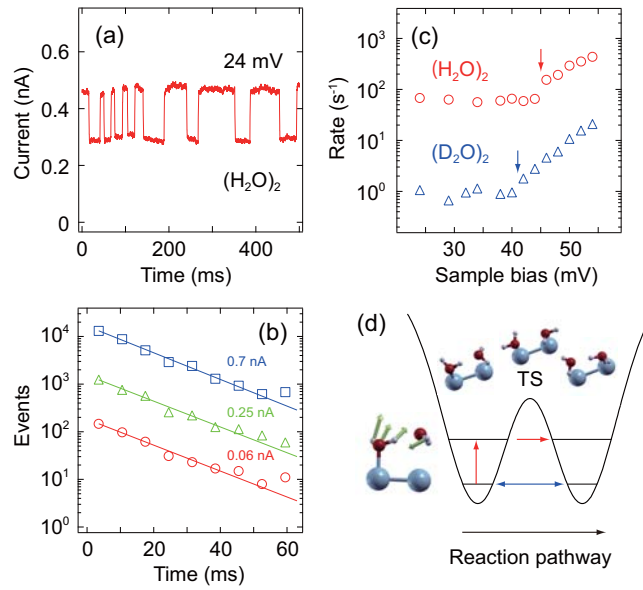
FIG. 8: (a) Typical tunneling current recorded with the tip fixed over the H_2O dimer (24 mV and 0.5 nA). The current jumps between the two states at the moments of the interchange reaction. (b) Distribution of the times for the dimer to stay at the two states. The slopes in semilogarithmic scale correspond to the interchange rates. The tip height is varied so that the current is kept at I=0.06 (red), 0.25 (green) and 0.7 nA (blue) for the high-current state. The latter two data are displaced vertically for clarity. (c) Voltage dependence of the interchange rate for H_2O dimer (red circles) and D_2O dimer (blue squares). The threshold voltages are 45±1 and 41±1 mV for $(H_2O)_2$ and $(D_2O)_2$, respectively (arrows). (d) A schematic diagram of the potential energy along the interchange reaction pathway. In addition to the intrinsic tunneling between the ground states (blue arrow), the interchange is assisted by the vibrational excitation of the donor-Cu stretch mode (the red arrows). (From [29].)
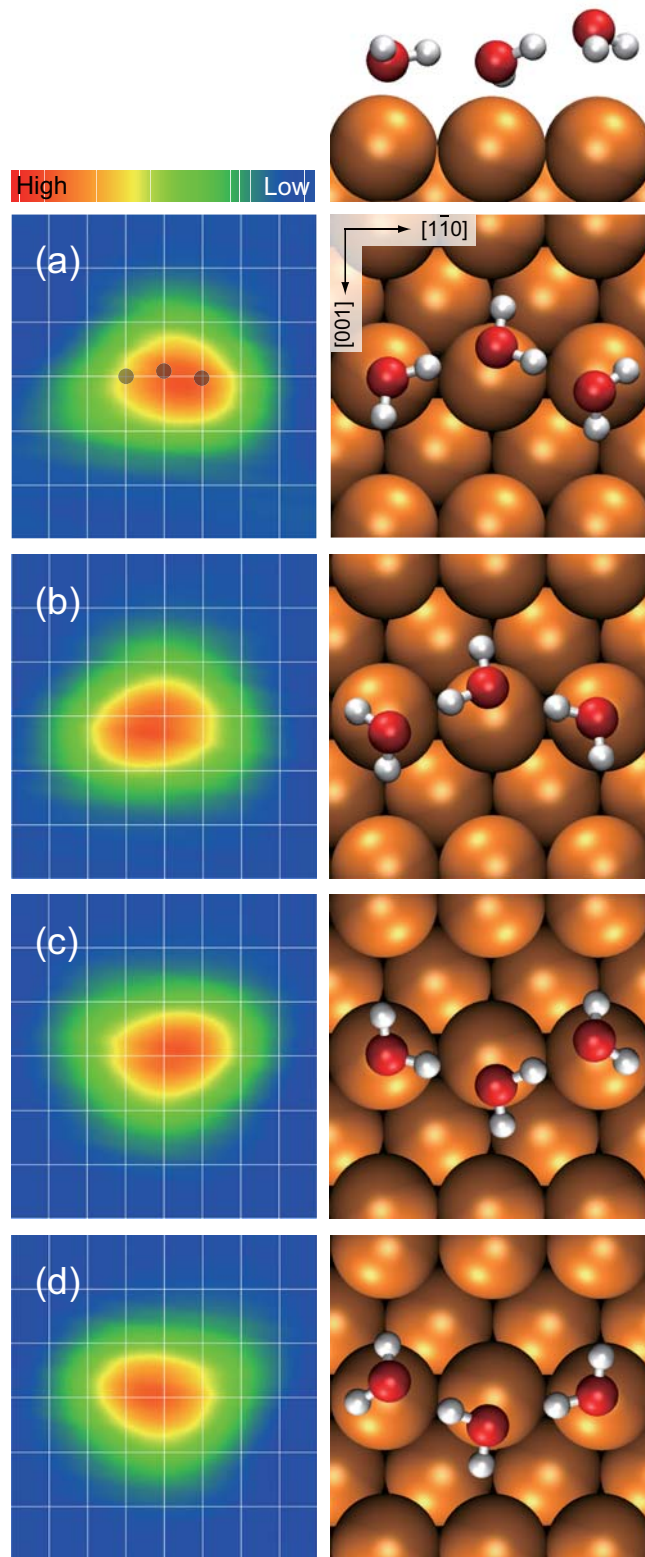
FIG. 9: (a)-(d) STM images of the chain trimer in four equivalent orientations, along with the corresponding structures obtained by DFT calculations. The lines represent the lattice of Cu(110), and the three dots in (a) depict the positions of water molecules. The trimer interconverts between the four orientations by 0.12 V voltage pulses. V_s=24 mV and I=0.5 nA (20×22 Å^2). (From [36].)

23
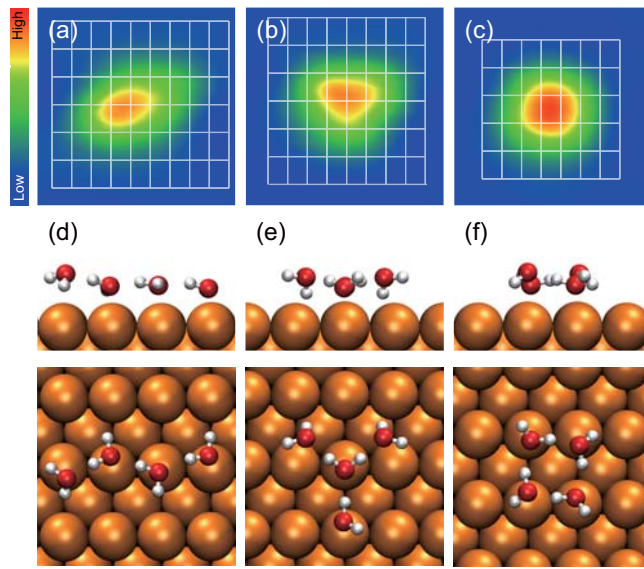
FIG. 10: STM images and optimized structures for water tetramers on Cu(110). (a)-(c) STM images of tetramers of chain, tetrahedral and cyclic types. (d)-(f) The corresponding structures optimized by DFT. The images are recorded at V_s=24 mV and I=2 nA (25×25 Å^2). The apparent height is 0.8, 0.8 and 1.0 Å for the images (a), (b) and (c), respectively. (From [36].)

24
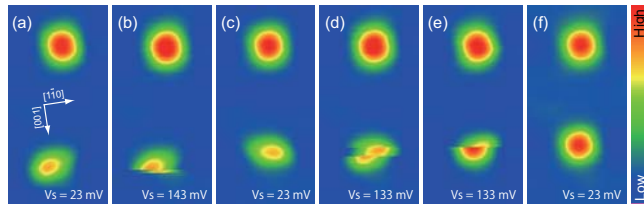
FIG. 11: Sequential STM images of two water tetramers on Cu(110) recorded with the bias voltage varied. The cyclic cluster (upper) is stable while the chain cluster (lower) flips between equivalent chain configurations at V_s=143 (133) mV [(b) and (d)]. The chain cluster eventually converts to the cyclic form in (e). The image size is $34{\times}67$ Å^2, and the tunnel current is 0.5 nA.

1
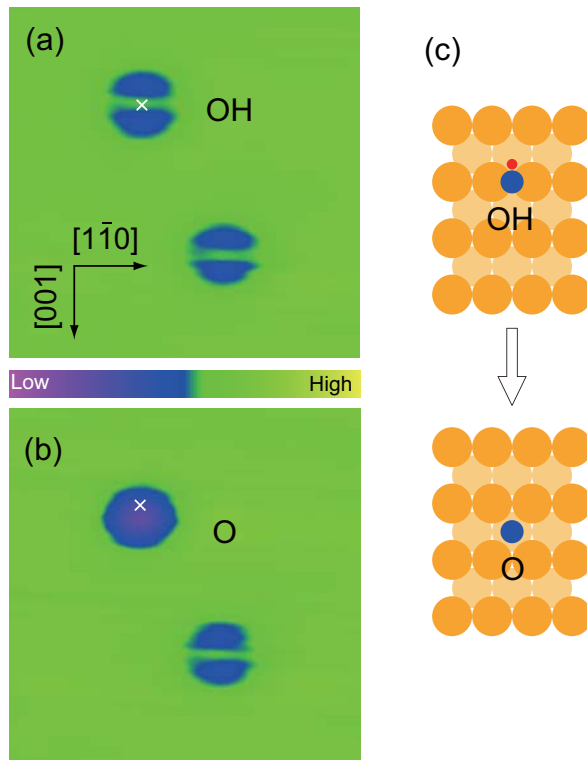
FIG. 12: Controlled dissociation of a OH group to an oxygen atom. (a) Two OH groups produced from two water molecules. The cross shows the center of an OH group (short-bridge site). (b) By applying a voltage pulse of 0.9 V, it turns into a round depression assigned as an oxygen atom. (c) The schematic illustration of the reaction. V_s=24 mV and I=0.5 nA (42×42 Å^2). (From [40].)
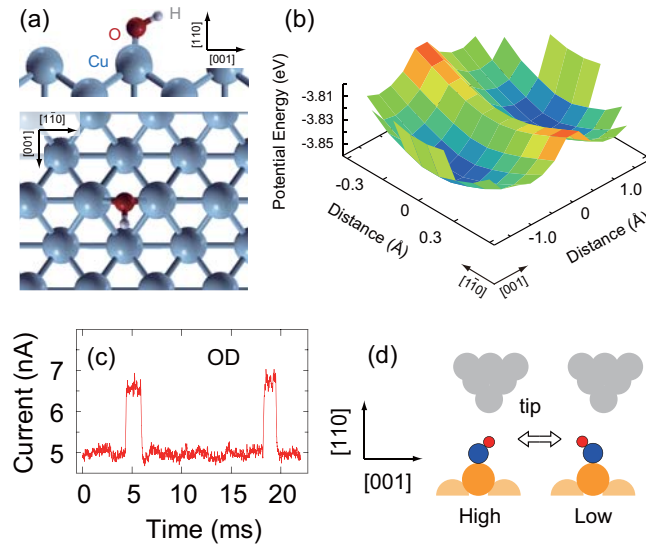
FIG. 13: (a) The structure of an OH group on Cu(110) obtained by DFT calculations. (b) Calculated potential energy surface of OH as a function of the lateral displacements of the H atom from the top of the bridge site. The two minima correspond to the inclined geometries, and the potential barrier to the flip motion is 0.14 eV. (c) Temporal evolution of tunneling current recorded with the tip fixed over one depression of OD. The two-state fluctuation corresponds to the back-and-forth flip motion of the inclined axis of OD. (d) Schematic illustration of the flip motion under the tip. The high-(low-)current state is tentatively designated as the orientation of D atom near (far from) the tip. (From [40].)

3
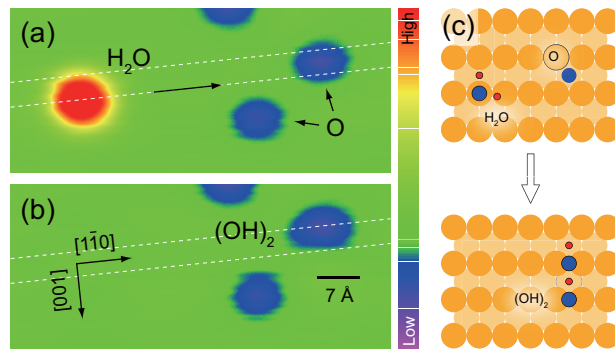
FIG. 14: Controlled reaction between a water molecule and an oxygen atom. The white dashed lines represent Cu rows of the Cu(110) surface. (a) A water molecule is dragged along the Cu row toward an oxygen atom. (b) They are encountered to yield an OH dimer imaged as a semicircular depression. The reaction occurs spontaneously when the two reactants come close to each other. (c) Schematic illustration of the reaction process. V_s=24 mV and I=0.5 nA.
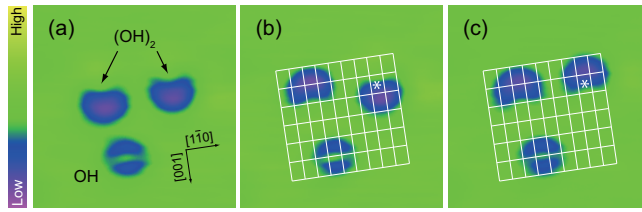
FIG. 15: (a) STM images of two OH dimers and one OH monomer. (b) The left dimer was flipped by a voltage pulse. (c) The right dimer was subsequently flipped in a similar way. The lines represent the lattice of the substrate, and the asterisks in (b) and (c) show the center of the flip motion that is located on the hollow site. The images were recorded at V_s=24 mV and I=5 nA (35×35 Å^2). (From [40].)
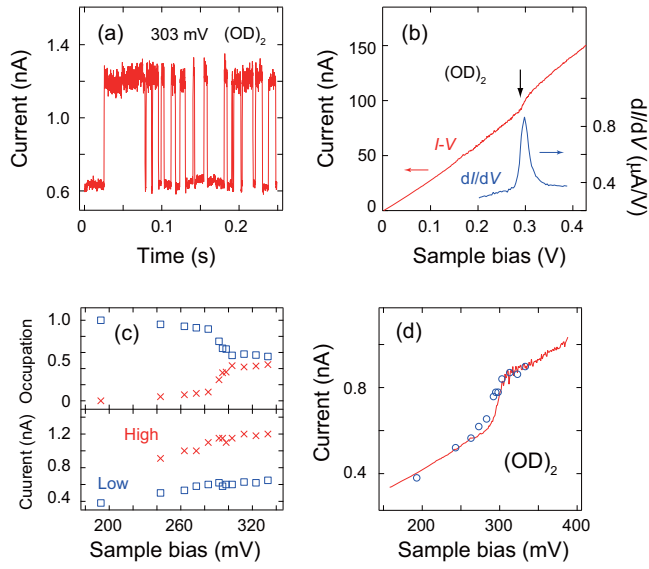
FIG. 16: (a) Temporal evolution of tunneling current recorded with the tip fixed over the depression of $(OD)_2$. The tip is fixed at the height corresponding to V_s=24 mV and I=0.05 nA, and then the voltage is increased to 303 mV. The two-state fluctuation corresponds to the back-and-forth flip motion of $(OD)_2$. (b) The current-voltage curve (I-V) recorded with the tip fixed over the depression of $(OD)_2$. The tip is fixed at the height corresponding to V_s=24 mV and I=5 nA, and the curve is the average of 60 scans. A non-linear feature is observed at $\sim$300 mV, which is clearly seen as a peak in the first derivative (dI/dV). (c) The state-resolved I-V plots (lower panel) and the fractional occupation (upper panel) for the low (squares) and high (crosses) states as a function of V_s for $(OD)_2$. The data are obtained with the tip fixed over the depression at V_s=24 mV and I=0.05 nA. (d) Averaged I-V curve obtained over the depression of $(OD)_2$ at the same height as (c) (solid curve). Using the data in (c), the averaged I-V data is calculated (circles), which well reproduces the experimental curve. (From [40].)
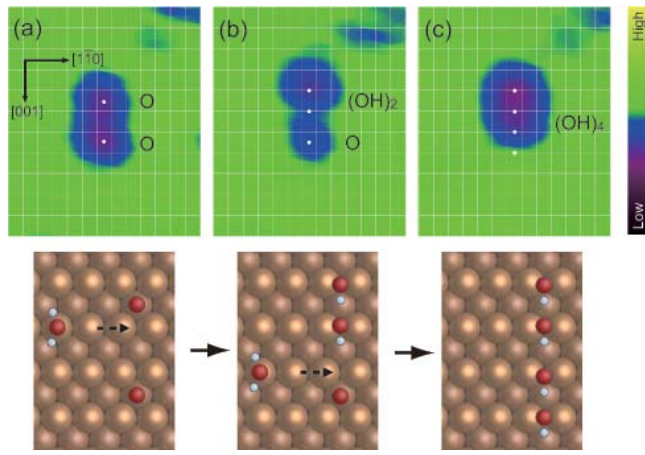
FIG. 17: The assembly process of $(OH)_4$. (a) Two oxygen atoms are adsorbed along [001] with the interval of $2b_0$. (b), (c) Two water molecules are successively brought to oxygen atoms, resulting in the formation of $(OH)_4$. The two-step reaction is schematically shown in the bottom. V_s=30 mV and I=0.2 nA (33×40 Å^2).
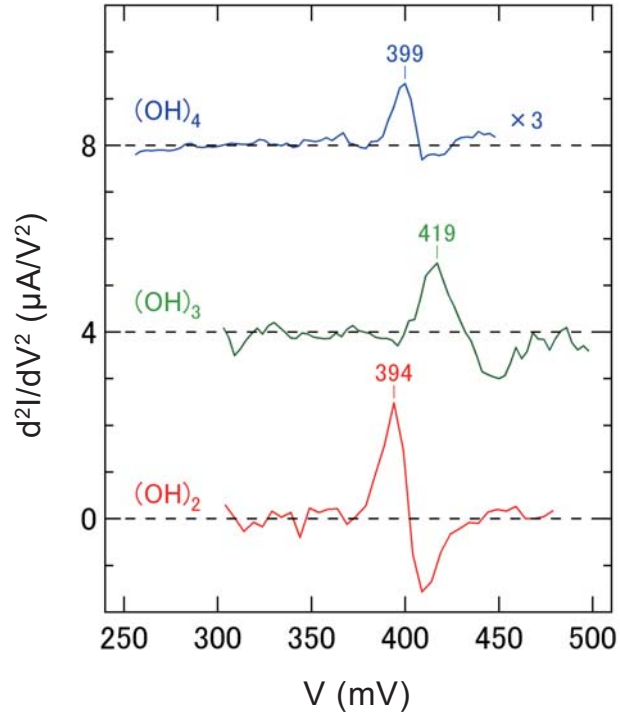
FIG. 18: d^2I/dV^2 recorded for (a) $(OH)_2$, (b) $(OH)_3$ and (c) $(OH)_4$. The tip is fixed over the depressions at the height corresponding to V_s=24 mV and I=0.5 nA for (a) and (c), and V_s=24 mV and I=0.05 nA for (b). The peak positions are independent on the tip height. The peaks are assigned to the vibrational excitation of the OH stretch. The trimer has higher frequency than the other two, indicating weaker H-bonding in the chain.
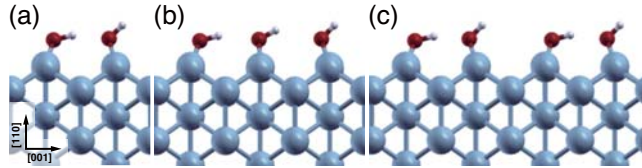

FIG. 19: The structures of (a) $(OH)_2$, (b) $(OH)_3$ and (c) $(OH)_4$ optimized by DFT.
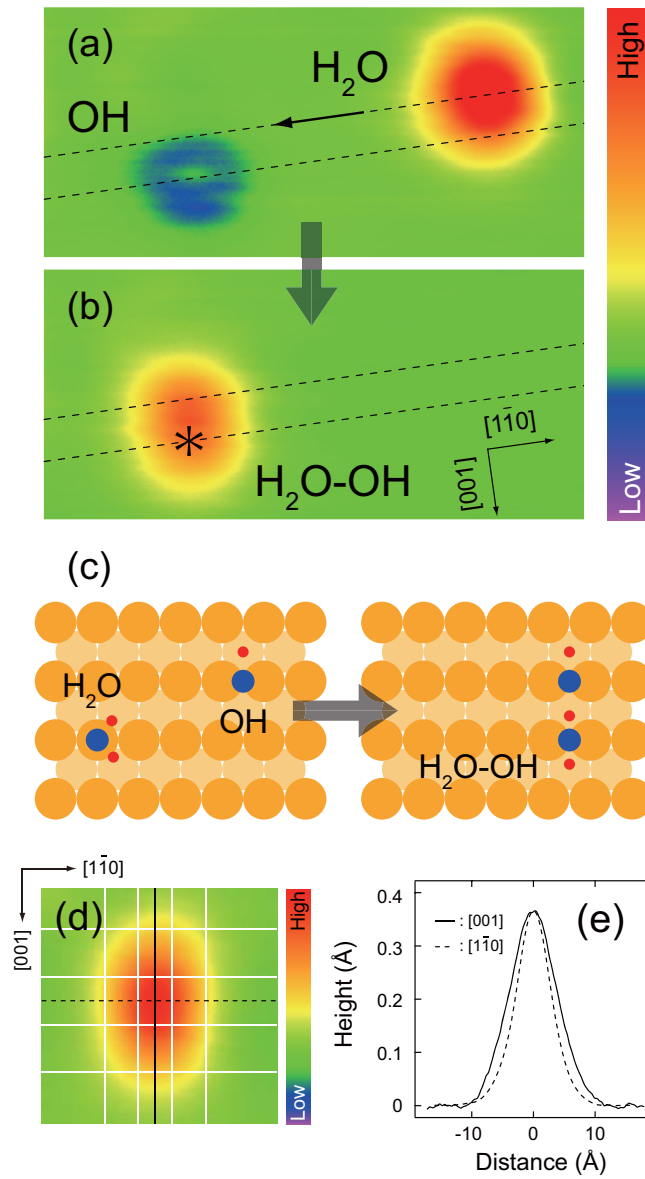
8

FIG. 20: STM images of a water molecule (right) and an OH group (left) located on the adjacent Cu rows (dashed lines). The water molecule is manipulated to react with the OH group along the arrow. (b) An image of the product that appears as an oval shape. (c) Schematic reaction between water and OH in (a)-(b). (d) An STM image of the product on which the lattice of Cu(110) is superimposed. (e) The height profiles along the solid ([001]) and dashed ([1$\bar{1}$0]) lines in (d). V_s=24 mV and I=0.5 nA for all images. The image size is $47{\times}22$ Å^2 for (a) and (b), and $17.5{\times}17.5$ Å^2 for (d). (From [50].)
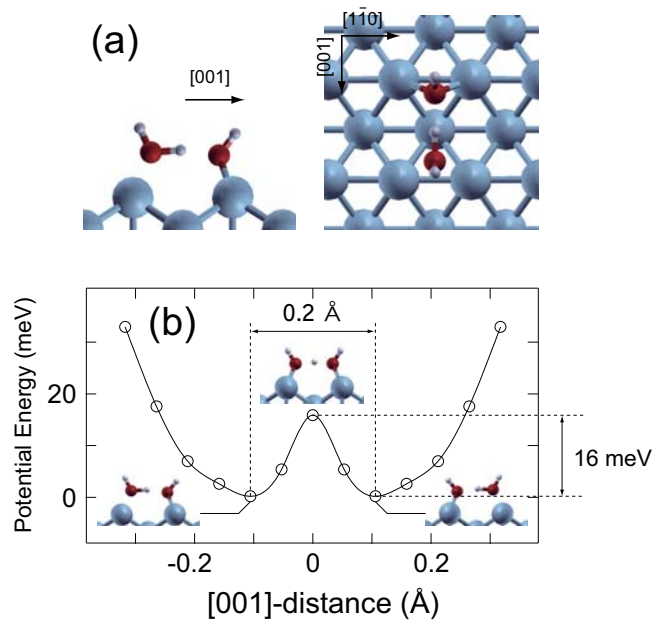
9

FIG. 21: (a) The most stable structure of the H_2O-OH complex obtained by the DFT calculation without zero-point-energy correction. (b) Adiabatic potential energy along the minimum-energy path of H-atom transfer between oxygen atoms (open circles). The two minima and peak correspond to the asymmetric and symmetric configurations, respectively, as shown in the inset. The energy difference between the asymmetric and symmetric structure is only 16 meV. The curve is obtained by a cubic spline fit to the calculated data. (From [50].)